TITLE:

The Kinase Module of the Mediator regulates cell cycle re-entry and transcriptional response following DNA damage

Gönen Memişoğlu[1,2*], Stefan Bohn[3], Nevan Krogan[4], James E. Haber[5], Alexander J. Ruthenburg [1,2,*]

[1] Department of Molecular Genetics and Cell Biology, The University of Chicago, IL, 60637, USA.

[2] Department of Biochemistry and Molecular Biology, The University of Chicago, IL, 60637, USA.

[3] Institute of Structural Biology, Helmholtz Zentrum München, Munich, GERMANY.

[4] Department of Cellular and Molecular Pharmacology, University of California, San Francisco, CA, 94158, USA.

[5] Department of Biology and Rosenstiel Basic Medical Sciences Research Center, Brandeis University, Waltham, MA, 02454, USA.

[*] Correspondence and requests for materials should be addressed to G. M. (email:gonen@uchicago.edu) or A. J. R. (email: aruthenburg@uchicago.edu)

ABSTRACT

When faced with a DNA double strand break, cells activate an elaborate signaling cascade called the DNA damage response to protect genomic integrity. To identify novel factors that modulate the DNA damage response to DNA double strand breaks, we performed an epistatic miniarray profile (E-MAP) analysis of Mec1 and Rad53, two essential kinases that coordinate the DNA damage response in budding yeast. Through this analysis, we discovered a genetic interaction between the kinase module (CKM) of the Mediator of transcription and Rad53. We find that all four subunits of the CKM, as well as CKM's kinase activity are critical for cell cycle re-entry following a DNA break, whereas the core Mediator subunits are dispensable. Notably, CKM mutants do not impair DNA repair by homologous recombination or confer sensitivity to DNA damaging reagents, suggesting that CKM specifically impinges on DNA damage signaling. In support of this, we find that Rad53 and CKM physically interact in response to DNA damage. Following the induction of a DNA break, CKM is a critical regulator of global transcription inhibition. In addition to this global effect, we illustrate that CKM functions locally at DNA breaks together with the core Mediator. In the absence of catalytically active CKM, the CKM-Mediator complexes at DNA breaks are replaced by RNAPII. Taken together, our results reveal a previously uncharacterized role for CKM in the DNA damage response.

INTRODUCTION

In budding yeast, a single DNA break is sufficient to activate an extensive DNA damage response and cell cycle arrest prior to anaphase (*1*). This response is entirely dependent on the Mec1 kinase (*2*) and is largely dependent on the downstream effector kinase Rad53 (*3*). Once

recruited to DNA breaks, Mec1 phosphorylates and activates Rad53 to initiate the DNA damage response and to ensure the inhibition of mitotic progression (*4*).

Mec1 and Rad53 are epistatic in several ways. First, both Mec1 and Rad53 are essential for viability (*5*), as they are required for the stabilization of replication forks under normal growth conditions (*6, 7*) and the inhibition of origin firing response to replication stress (*2, 8*). The lethality of either *mec1Δ* or *rad53Δ* cells can be rescued by the upregulation of the dNTP metabolism (i.e., by the deletion of ribonucleotide reductase inhibitor *SML1* (*9*)). Moreover, both *mec1Δ sml1Δ* and *rad53Δ sml1Δ* cells are hypersensitive to DNA damaging reagents, such as alkylating reagent MMS (*7*). Additionally, phosphoproteomics studies show that the protein targets of Mec1 and Rad53 significantly overlap (*10, 11*).

However, recent genetic and biochemical evidence implies that Rad53 also has Mec1-independent functions. For instance, Rad53 prevents excess histone accumulation (*12, 13*) and binds to promoter sequences (*14*) independently of Mec1. Furthermore, a recent report suggests that Rad53 can oligomerize and autophosphorylate in response to DNA replication stress in the absence of the upstream DNA damage kinases Mec1 and Tel1 (*15*).

To systematically investigate Mec1-independent functions of Rad53 and discover previously uncharacterized regulators of DNA damage response, we undertook a quantitative epistatic miniarrray profile (E-MAP) screen (*16, 17*). The E-MAP screen relies on creating permutations of a haploid query mutant strain by crossing it to the entire haploid yeast deletion library through sporulation, tetrad dissection and selection. The colony sizes of the resulting strains are quantified and assigned positive or negative scores as a proxy of improved or worsened growth in the double mutants with respect to the single mutants. Further analysis of these comparative growth scores reveals genes which are epistatic to the query mutation to differing extents.

Our E-MAP analysis of *RAD53* and *MEC1* unveiled a previously uncharacterized interaction between *RAD53* and various subunits of a large protein complex called the Mediator of transcription. The Mediator is a multi-subunit protein complex which functions as a general transcription factor by bridging RNA polymerase II (RNAPII) and DNA-bound transcription factors (*18*). The core Mediator contains at least 21 highly-conserved subunits grouped into head, middle and tail modules (*19, 20*), and regulates essentially all RNAPII-dependent transcription by binding to transcriptional complexes. The core Mediator can also reversibly associate with an accessory Cdk8 Kinase Module (CKM) (*21*), which consists of Cdk8 kinase, CycC, Med12 and Med13 in equimolar composition (*22, 23*). CKM has been generally regarded as a transcriptional suppressor (*24*); however, recent studies suggest a context-dependent role

for CKM both in transcriptional activation and repression (*25, 26*). Structural analysis shows that the core Mediator-CKM and core Mediator-RNAPII interactions are mutually exclusive, supporting the findings which characterize CKM as a transcriptional suppressor.

Here, after identifying a specific genetic interaction between Rad53 and CKM, we explored the role of CKM in the context DNA damage response in depth. Our results illustrate that all four CKM subunits and the enzymatic activity of CKM are required for cell cycle reentry following a DNA break whereas the core Mediator and components of the general RNAPII-dependent transcription are dispensable. Our bulk RNA-sequencing analysis with CKM conditional depletion illustrate that DNA damage triggers a CKM-dependent transcriptional downregulation. We find that CKM evicts RNAPII to antagonize transcription at sites of DNA damage and globally to downregulate transcription. Lastly, we show that DNA damage leads to an increase in CKM abundance and nuclear localization. We posit that upon activation of DNA damage signaling, CKM is upregulated and recruited to the nucleus to counteract local and global transcription complexes and function to facilitate cell cycle reentry.

RESULTS

An epistatic miniarray screen reveals a genetic interaction between RAD53 and the Mediator kinase module

To explore additional factors that regulate the cellular responses to DNA damage, we performed an E-MAP analysis (*17*) of *rad53Δ sml1Δ* and *mec1Δ sml1Δ* mutants, by using a *sml1Δ* mutant as a WT control as previously described (*27*) [Figure 1A]. The E-MAP screen revealed that under normal growth conditions, *RAD53* and *MEC1* phenotypic signature scores, also referred to as CC scores, significantly overlap; especially for targets that are involved in DNA damage response such as checkpoint clamp subunits *RAD17* and *RAD24* (*28*) and the DNA damage response adaptor *RAD9* (*29*) [Figure 1B]. Surprisingly, among the top genes that yield similar phenotypic signature scores with *RAD53*, we find subunits of the Mediator of transcription [Figure 1C], a multi-subunit protein complex that functions as a general transcription factor to regulate RNAPII (*18*). Some of these interactions, such as the CDK8 Kinase Module (CKM) subunits *CDK8*, *CYCC*, *MED13* and *MED12* are specific to *RAD53* whereas the middle Module subunits *MED1* and *MED9* display a strong correlation with both *RAD53* and *MEC1* [Figure 1B].

To test whether the CKM of the Mediator and *RAD53* function in parallel to regulate growth under normal conditions and to confirm the findings of the E-MAP screen, we created diploid yeast strains containing *rad53-K227A* (*30*), *mec1-D2224A* (*31*) and *cdk8-D304A* (*32*)

kinase-dead mutations (hereafter referred to as *kd*) via CRISPR/Cas9 (*33*). In addition, we introduced a compensatory *sml1Δ* mutation to prevent the lethality of *rad53-kd* and *mec1-kd* (*9*). We dissected tetrads from sporulated diploid mutants and quantified the resulting colony sizes of single and double mutants. The *rad53-kd cdk8-kd* double mutant colonies are significantly smaller than WT or the single *rad53-kd* and *cdk8-kd* mutant colonies, suggesting that CKM and Rad53 function in parallel, and that their kinase activities are both critical for growth [Figure 1D]. Conversely, *mec1-kd cdk8-kd* double mutants do not exhibit a synergistic growth defect, confirming our initial findings from the E-MAP screen. These results point to a surprising functional link between the kinase module of the Mediator of transcription (CKM) and Rad53, the effector kinase of the DNA damage response.

CKM mutations cause defects in the DNA damage response

Given its strong interaction with *RAD53* in growth assays, we posited that the kinase module of the Mediator could regulate the DNA damage response. The induction of a single irreparable DNA double strand break causes an extended G2/M arrest prior to anaphase in yeast (*1*). However, 12 to 15 hours after the induction of a DNA break, cells eventually extinguish the DNA damage signaling and resume cell cycle through a process called "adaptation" (*34*). To test whether the CKM impacts G2/M arrest and adaptation, we created a collection of Mediator mutants in a strain that contains a galactose-inducible HO endonuclease, which induces a single and irreparable DNA break at the *MATα* locus (*1*). We picked G1 cells on galactose containing plates by micromanipulation to induce an irreparable break and followed their cell cycle progression at regular time intervals. As expected, nearly all WT cells were arrested by 8 hours and nearly all cells were adapted by 24 hours [Figure 2A]. Mutants of subunits from the core Mediator head (*med18Δ* and *med20Δ*) and tail (*med2Δ* and *med16Δ*) arrested and adapted like WT [Figure 1A] with slight cell cycle arrest defects at 8 hours. Interestingly, we observe a slight adaptation defect with the middle module mutants *med1Δ* and *med9Δ*. In contrast, the CKM mutants *med12Δ, med13Δ, cyccΔ* and *cdk8Δ* as well as *cdk8-kd* were unable to adapt at 24 hours. These findings indicate that the severe adaptation defects are specific to the CKM module mutants within the Mediator complex.

To examine whether the adaptation defect of CKM mutants is independent of the modality of DNA damage induction, we sought alternate means of triggering the DNA damage signaling. To this end, we employed a temperature sensitive *cdc13-1* mutant, which causes telomere uncapping and consequently, the activation of DNA damage response at nonpermissive temperatures (33°C) (*35*). The *cdc13-1* mutant cells were mostly arrested 8 hours after switching to nonpermissive temperature but adapted by 24 hours; whereas *cdc13-1 cdk8-kd* double mutants failed to adapt. Taken together with the results from the adaptation

assay above, these findings illustrate that the kinase activity of CKM is required for proper cell cycle re-entry following the extended G2/M arrest.

To complement these functional assays, we investigated the molecular read-outs of DNA damage signaling and adaptation. Rad53 is maintained at a hyperphosphorylated state throughout the extended DNA damage induced cell cycle arrest and is gradually dephosphorylated as the cells adapt (*36*). We monitored Rad53 hyperphosphorylation in CKM mutants as compared to core Mediator mutants following the induction of a single irreparable DNA break with western blotting to test whether the adaptation defect of CKM mutants translates to an increase in Rad53 hyperphosphorylation. In WT cells, we detect hyperphosphorylated Rad53 species 8 hours after the induction of a single DNA break, which becomes fully dephosphorylated by 24 hours as the cells re-enter mitosis. In middle, head, and tail module mutant cells, we detected WT-levels of Rad53 hyperphosphorylation in response to DNA damage, and a complete Rad53 dephosphorylation at 24 hours as cells turn off the DNA damage signaling [Figure 2C, D]. We find similar Rad53 phosphorylation responses for essential core Mediator subunits upon auxin-inducible depletion (AID) [Figure 4D]. However, in CKM mutants *med12Δ* and *med13Δ*, Rad53 hyperphosphorylation persists up to 24 hours, agreeing with the adaptation assay results pointing to a defect in cell cycle re-entry [Figure 2C]. To evaluate the kinetics of Rad53 activation and deactivation in response to DNA damage with higher temporal resolution in these mutants, we assayed Rad53 hyperphosphorylation in WT, *med1Δ* and *med13Δ* cells at 3 hour intervals over the course of 24 hours. After the induction of a DNA break in both WT and *med1Δ* cells, we found Rad53 was hyperphosphorylated around 6 hours followed by the gradual dephosphorylation [Figure 2D]. However, both in in *med13Δ* mutant, we detect residual hyperphosphorylated Rad53 persisting up to 24 hours. These results illustrate that CKM function, but not core Mediator, is required for a timely inactivation of DNA damage signaling and resumption of mitosis.

Deletion of CKM subunits alter gene expression (*37*). Hence, the effect of CKM on DNA damage response could be an indirect consequence of changes in transcription which stem from loss of CKM for several generations. To define the proximate role of CKM on DNA damage signaling, we employed the auxin-inducible degron (AID) strategy (*38*) to deplete Med12 6 hours after the induction of DNA damage. Our results demonstrate that acute Med12 depletion is sufficient to elicit an increased DNA damage response, evident from the accumulation of hyperphosphorylated Rad53 species at 24 hours [Figure 2E]. To support these findings, we also created an analog sensitive *cdk8-Y236G* (*39*) (hereafter referred to as *cdk8-as*), which can be selectively inhibited by using large ATP analog 1-Naphthyl-PP1 (1-NA-PP1). The treatment of *cdk8-as* mutant with 1-NA-PP1 following DNA damage also led to an accumulation of hyperphosphorylated Rad53 species at later time points [Figure 2F]. These data show severe

DNA damage signaling defects at both functional and molecular level observed for all four CKM subunit mutants are unique to this module of the Mediator complex and rely on its kinase activity.

CKM mutants do not impair DNA repair

After establishing the function of CKM on DNA damage response following an irreparable break, we investigated the role of CKM on DNA repair by homologous recombination. We introduced CKM mutations in a YJK17 strain [Figure 3A], in which a DNA break on chromosome III is repaired by using the ectopic donor sequence on chromosome V via gene conversion (GC) (*40*) within 8 hours without a pronounced cell cycle arrest (*41*). The viability of these mutants following DNA damage was comparable to WT [Figure 3B]. To assay the gene conversion repair kinetics and DNA damage response during repair in parallel, we introduced a *cdk8-as* mutation in YJK17 strain, inhibited CKM activity by 1-NA-PP1 treatment, quantified the formation of the repair product by PCR (*42*) and examined Rad53 hyperphosphorylation by western blotting. These data demonstrate that CKM inhibition leads to a small, but reproducible, improvement in initial repair kinetics, however, does not alter the final repair efficiency, supporting the viability assay results [Figure 3C]. In contrast with a strain where homologous repair templates are absent and therefore, the DNA break is irreparable [Figure 2D], Rad53 phosphorylation kinetics with or without CKM inhibition are comparable in YJK17 strain [Figure 3D], illustrating that CKM function is dispensable for both DNA repair and the DNA damage signaling following a brief cell cycle arrest.

Next, we employed YMV80 single strand annealing (SSA) strain (*36*) in which a DNA break induced between two homologous sequences interrupted by a 25 kb insertion is repaired after extensive 5' to 3' resection of the 25 kb region [Figure 3E]. This SSA event takes approximately 12 hours to repair and evokes the DNA damage response. The CKM subunit mutants did not alter the viability in YMV80 [Figure 3F]. As opposed gene conversion repair kinetics, inhibition of CKM kinase activity in a *cdk8-as* mutant with 1-NA-PP1 treatment did not significantly alter repair kinetics or the percentage of repair product at 24 hours [Figure 3G]. However, the inhibition of CKM led to a noticeable increase in Rad53 hyperphosphorylation, especially at later time points [Figure 3H]. Collectively, these findings demonstrate that CKM is dispensable for homologous recombination by gene conversion and single strand annealing, but is critical for extinguishing DNA damage signaling, especially as the cells resume mitosis following an extended G2/M arrest.

Core Mediator subunit Med17 is involved in nucleotide excision repair in response to UV damage (*43, 44*); however, the role of CKM in UV damage response has not been studied. To test this, we performed a spot assay with a *cdk8-kd* strain, along with *mec1-kd* and *rad53-kd* as

controls. Our results indicate that *cdk8-kd* mutants are not sensitive to UV levels which are lethal to *mec1-kd* cells [Figure 3I]. Moreover, *cdk8-kd* mutation does not further sensitize the *rad53-kd* to UV, indicating that CKM is dispensable for nucleotide excision repair. Interestingly, we observe that the UV sensitivity of *mec1-kd* was slightly alleviated by *cdk8-kd*. We also tested the sensitivity of *cdk8-kd* cells to hydroxyurea (HU), which causes stalled replication forks. Rad53 and Mec1 kinase activities are essential for the stabilization of replication forks (*6, 7*), and therefore, both *rad53-kd* and *mec1-kd* cells are sensitive to HU [Figure 3I]. The *cdk8-kd* mutant is not sensitive to low HU concentrations, however, it alleviates the HU sensitivity of *rad53-kd* and *mec1-kd* mutants, presumably by strengthening the checkpoint response. Taken together, these results demonstrate that CKM specifically impinges on DNA damage signaling and does not significantly alter DNA damage repair.

CKM contributes to the global downregulation of transcription in response to DNA damage

Given the function of CKM in transcriptional regulation (*18*), we hypothesized that CKM could alter the DNA damage signaling by altering the transcriptional responses to DNA damage. To examine this possibility, we performed a bulk RNA sequencing experiment in a Med12-AID strain to inhibit CKM activity. In accord with previously published studies illustrating that CKM depletion does not markedly alter the transcriptome with only a slight global upregulation (*37, 45*), our results show that even after 10 hours of CKM depletion, changes in global transcription are modest [Figure 4A, B]. In contrast, we observe a pronounced downregulation of transcription following the induction of a single DNA break. Remarkably, we find that that this global downregulation is largely dependent on CKM activity, as the AID depletion of CKM subunit Med12 blunts the downregulation at many of the damage-regulated target genes. These data suggest a more prominent role for CKM activity in the global downregulation of transcription in response to DNA breaks as compared to its more modest impact on general transcription under normal conditions.

In response to DNA damage by UV, cells shut down transcription by ubiquitylation and subsequent degradation of RNAPII (*46*). To address whether the DNA-damage dependent downregulation of transcription in response to a single DNA break regulates transcription through a similar pathway, we monitored the protein abundance of core transcriptional machinery by western blotting [Figure 4C]. We do not detect any changes in core Mediator subunit Med1 or RNAPII subunit Rbp3, nor do we detect changes in of active RNAPII complexes marked by RNAPII-S2P and RNAPII-S5P following DNA damage [Figure 4B]. Additionally, inhibition of CKM activity in a *cdk8-as* strain did not alter the abundance of core transcription machinery or the active RNAPII pools. Collectively, these results indicate that the drastic transcriptomic changes in response to a single DNA break is not due to the degradation or

modification of core transcriptional machinery, and CKM plays an active role to shut down transcription.

Next, to test whether the cell cycle re-entry defect of CKM mutants could be due to the absence of complete transcriptional downregulation, we created conditional mutants of the essential transcriptional machinery to synthetically downregulate transcription. Loss of Med14 is shown to cause dissociation of all core Mediator modules, whereas the depletion of Sua7 impairs the pre-initiation complex assembly (*47, 48*). AID depletion of both of these proteins significantly downregulate transcription (*49*). In WT cells, AID depletion of Med14 or Sua7 slightly impaired the Rad53 hyperphosphorylation following a single DNA break, especially evident at 4 hours after DNA damage [Figure 4C]. However, when combined with a *cdk8-kd* mutant, the depletion of Med14 or Sua7 completely abolished Rad53 hyperphosphorylation [Figure 4D]. Together, these results demonstrate that DNA damage response relies heavily on transcription, and CKM also plays an essential and transcription-dependent role in maintaining the cell cycle arrest in response to DNA damage.

CKM limits chromatin-bound RNAPII pools to inhibit transcription following DNA damage

We find that DNA damage leads to global downregulation of transcription without altering the abundance of essential transcriptional proteins. Therefore, we hypothesized that chromatin bound RNAPII pools might be altered in response to DNA damage. To test this, we measured RNAPII occupancy at four control loci with varying levels of Cdk8, CycC and RNAPII enrichment (*50*) and gene lengths varying between 500 bases to 2kb by using chromatin immunoprecipitation after DNA damage induction. In WT cells, we observe a steady decrease in RNAPII occupancy at all four loci as a function of time after DNA damage independent of gene length, CKM, core Mediator and RNAPII occupancy [Figure 5A]. This decrease was entirely reversed when we inhibit CKM kinase activity in a *cdk8-as* mutant with 1-NA-PP1 treatment. Taken together with the CKM-dependent global downregulation of transcription, these results suggest that CKM kinase activity is critical for eviction of RNAPII from chromatin to antagonize transcription in response to DNA damage.

We find that DNA damage leads to a CKM-dependent reduction in chromatin bound RNAPII pools and consequently, a downregulation of global transcription without altering the abundance of core transcriptional machinery. Therefore, we posited that CKM activity might be altered upon DNA damage to achieve a damage-dependent decrease in transcription. To monitor changes to CKM subunit stoichiometry and kinase activity, we created a yeast strain in which all the in which all four CKM subunits are appended with epitope tags. First, we assayed the changes in CKM subunit abundance from cell lysates in this strain following DNA damage by western blotting. We observe that DNA damage leads to an upregulation of all four CKM

subunits, which is consistent with the previously published *in vitro* assays suggesting that CKM has equimolar subunit composition (*23*). We note a significant decrease in CKM abundance at 24h both in cycling and DNA damage-treated cultures, and we deduce that CKM levels could be downregulated in response to cellular crowding. Next, we assayed changes in inter and intramolecular CKM interactions by Cdk8-FLAG and Med13-myc coimmunoprecipitation analyses. Although the abundance of individual CKM subunits vary across conditions and at different times, the CKM subunit composition does not change significantly in response to DNA damage [Figure 5C]. However, we detect an enrichment of CKM binding to RNAPII, specifically after DNA damage signaling is activated. Notably, we find that at least a portion of CKM-bound RNAPII is S5 and S2 phosphorylated (*51*). Given that CKM is shown to phosphorylate RNAPII C-terminal repeats at S2 and S5 (*32, 52*), these findings imply that CKM's kinase activity is stimulated upon DNA damage. We also note that we find a weak interaction between Rad53 and Med13 specifically following DNA damage, confirming the previously published results illustrating that genetic interactions identified through E-MAP screen generally also translate to physical interactions (*53*). These findings raise the possibility of CKM being modified by DNA damage kinases such as Rad53, which, in turn regulate CKM function.

CKM functions locally at DNA break sites

To test whether CKM functions directly at DNA breaks together with Med1 and RNAPII to regulate DNA damage signaling, we constructed a strain in which core Mediator subunit Med1, RNAPII subunit Rbp3 and CKM kinase Cdk8 are tagged with epitope tags [Fig 4C], performed chromatin immunoprecipitation and analyzed the resulting DNA fragments by qPCR. As a control, we analyzed the enrichment and spreading of the DNA damage dependent histone mark γ-H2AX (*54*) around DNA breaks in WT and *cdk8-as* sensitive cells treated with 1-NA-PP1. Neither the spreading nor the enrichment of γ-H2AX was altered in upon CKM inhibition [Figure 6]. In WT control cells, we detect a DNA damage dependent Med1 and Cdk8 enrichment around DNA breaks, while RNAPII is excluded from the break site throughout the time course experiment [Fig 6A, left]. However, inhibition of CKM kinase activity with 1-NA-PP1 treatment in the *cdk8-as* mutant leads to a loss of DNA damage dependent Cdk8 and Med1 binding to DNA breaks. Notably, the absence of Cdk8 and Med1 enrichment at DNA breaks leads to increased RNAPII recruitment at DNA breaks as a function of time [Figure 6A, right], and follows the RNAPII enrichment trend we detect at the control loci [Figure 5A]. These findings illustrate that CKM functions both locally at the break site and globally to evict active RNAPII complexes and antagonize transcription.

CKM kinase activity and DNA damage localization regulates the nuclear localization of CKM

After establishing that CKM and core Mediator localizes to DNA breaks, we asked whether DNA damage alters the cellular localization of CKM and core Mediator subunits. To this end, we

created fluorescently tagged Med17, Cdk8 and CycC strains and assayed the changes in protein localization by live cell imaging. As expected, under basal conditions in WT strains, all Mediator subunits localize to the nucleus [Figure 6B, first panel]. Following the induction of a single DNA break, we detect an enrichment in nuclear localization of all CKM subunits tested, illustrating that DNA damage signaling regulates the localization of Mediator subunits [Figure 6B, second panel]. This effect was more pronounced with CKM subunits Cdk8 and CycC, agreeing with the increase in CKM subunit protein abundance in response to DNA damage [Figure 5B].

Notably, in the absence of Cdk8 kinase activity, CKM subunits Cdk8 and CycC as well as the core Mediator subunit Med17 show increased vacuolar localization [Figure 6B, third panel]. This could be indicative of an increased CKM complex degradation in the absence of CKM catalytic function. In fact, we also observe a decrease in Cdk8, CycC and Med12 abundance following auxin-inducible depletion of Med13 [Figure 5B]. Taken together, these findings suggest that CKM abundance and localization are tightly regulated to fine-tune transcription in response to environmental cues such as DNA damage.

DISCUSSION

Although so far, Rad53 has been mostly regarded as a downstream target of the upstream kinase Mec1, evidence from recent studies imply that Rad53 also carries out Mec1-independent functions (*12, 14, 15*). Here, through an unbiased and quantitative genetic screen, we identified a genetic interaction between the CKM of Mediator of transcription and Rad53 and mostly focused on the role of CKM on DNA damage response to a single DNA break, which is orchestrated exclusively by Mec1. However, our tetrad analysis with catalytically-dead Cdk8, Rad53 and Mec1 strains as well as the E-MAP interaction data point to a possible DNA damage and Mec1-independent interaction between Rad53 and CKM, which is yet to be identified. We posit that CKM and Rad53 function in parallel to resolve the conflicts between replication and transcription under replication stress. Supporting this hypothesis, a recent paper finds that in response to replication stress Rad53 binds to the promoters of a diverse set of genes without sequence specificity and independently of DNA damage signaling (*14*). CKM could interact with Rad53 to mediate its recruitment to chromatin. In fact, our data show a DNA damage-induced physical interaction between CKM and Rad53. Alternatively, CKM might be essential for limiting transcription in response to replication stress by dampening RNAPII and allowing Rad53 recruitment. Future work will focus on the DNA damage-independent aspect of CKM-Rad53 interaction.

Recent structures suggest that the CKM and core Mediator interactions are facilitated by the middle module subunits (*45, 55*). Additionally, we observe that *MED1* and *MED9* have high E-MAP CC scores both for *RAD53* and *MEC1* [Figure 1B]. Based on these results, we conjecture

that this slight adaptation defect observed in *med1Δ* and *med9Δ* cells could be due to impaired CKM-core Mediator binding.

In vitro analysis of CKM suggest that CKM's binding to core Mediator sterically hinder core Mediator's binding to RNAPII (*45*). Remarkably, this steric hinderance is independent of the kinase activity of CKM. Contradicting this, our chromatin immunoprecipitation data suggest that RNAPII occupancy on chromatin in response to DNA damage is affected by the kinase activity of CKM. We postulate that CKM's kinase activity might play an indirect role on its transcriptional function. Our confocal live cell imaging results illustrate that CKM's kinase activity is required for the proper nuclear localization of the complex. Moreover, in the absence of CKM's kinase activity, we observe a reduction in CKM abundance. These results suggest that the catalytic activity of CKM could alter its transcriptional function by altering the localization and abundance of the complex.

In addition to the regulation of DNA damage via CKM, we also have evidence to suggest that CKM is modulated by the DNA damage signaling. We detect an upregulation of CKM subunit abundance and a concordant increase in nuclear CKM by confocal live cell imaging in response to DNA damage. Furthermore, we find that CKM is recruited to DNA breaks and interacts with the DNA damage kinase Rad53. Lastly, our coimmunoprecipitation analysis of the Cdk8 kinase domain imply an increase in CKM kinase activity specifically in response to DNA damage.

Collectively, our results indicate that CKM is critical for DNA damage response in budding yeast. Since the structure and function of CKM is highly conserved from yeast to mammals, we predict that CKM might also be involved in regulation of DNA damage response in mammalian cells. In fact, CKM has been associated with various cancers (*56, 57*). Moreover, two recent studies identified CKM as a suppressor of ATR (human Mec1 ortholog) inhibitor in genome wide screens (*58, 59*). Akin to the role of CKM we describe in DNA damage response, the ATRi resistance function of Med12 in mammalian cells is independent of the core Mediator (*58*). Additionally, CKM is shown to interact with DNA-dependent serine threonine kinase DNA-PK, which is a regulator of mammalian DNA damage response as an interaction partner of CKM (*23*).

FIGURE LEGENDS

Figure 1. A. Workflow of the epistatic miniarray profiling (E-MAP) screen. Query yeast strains *rad53Δ sml1Δ*, *mec1Δ sml1Δ*, as well as the WT control *sml1Δ* strains were systematically crossed to the yeast deletion library and automatically plated. Resulting colony sizes were used

to infer the alleviating or aggravating interactions for *RAD53* and *MEC1* in this growth assay. **B.** The heatmap representing the phenotypic signature scores (CC scores) for a WT control, *RAD53* and *MEC1*. Notable interactions are shown below. **C.** Illustration of yeast Mediator complex adapted from Guglielmi *et al* (*60*). **D.** Representative analysis of tetrads obtained from catalytically inactive mutant crosses: *rad53-kd cdk8-kd and mec1-kd cdk8-kd* double mutant diploids (left). All strains contain compensatory *sml1Δ* mutants. Colony sizes were quantified and plotted after 2 days of growth on YEPD plates (right), lines indicate mean colony size for the condition (n>5).

Figure 2. A. Adaptation assay results for Mediator head, middle, tail and CKM mutants. For each experiment, 50 G1 cells were micromanipulated on agar plates. The percentage of adapted cells were scored at 8h, 24h and 48h after the induction of DNA damage (n>3; error bars represent S.E.M.; *** $p<0.001$, 2-way ANOVA). **B.** Adaptation assay, as in panel 1A, with *cdc13-1* temperature sensitive mutants at permissive (25^0C) and non-permissive (33^0C) temperatures (n>3; error bars represent S.E.M.; *** $p<0.001$, 2-way ANOVA). **C.** Rad53 hyperphosphorylation in Mediator mutants after DNA damage by HO-endonuclease induction by western blotting. **D.** A finer grained time course of Rad53 hyperphosphorylation in select Mediator mutants after DNA damage by HO-endonuclease induction. **E.** Rad53 hyperphosphorylation in *cdk8-as* mutant treated with 10 μM 1-NA-PP1 ATP analog, applied 4 hours after the induction of DNA damage by HO-endonuclease. **F.** Rad53 hyperphosphorylation following Med12-AID depletion by the addition of auxin at a final concentration of 100 μM (IAA), at 6 hours after the induction of DNA damage. Samples were blotted for myc to monitor Med12-AID depletion, and for Pgk1 as loading control.

Figure 3. A. A schematic representation of the YJK17 gene conversion repair strain (*40*). The HO-induced DNA break on Chromosome III at *MAT*α locus is repaired by using the *MAT*a-*inc* ectopic donor sequence on chromosome V, which contains an *-inc* mutation to prevent continuous cutting. After DNA repair is complete, *MAT*α sequence is replaced by *MAT*a-*inc*. **B.** The viabilities of CKM deletion mutants in YJK17 strain background strains following DNA damage (n=3, error bars represent S.E.M.). **C.** DNA repair kinetics measured by primer extension assay in YJK17 *cdk8-as* mutant with and without 20 μM 1-NA-PP1 treatment (n=3; error bars represent S.E.M). **D.** Rad53 hyperphosphorylation following DNA damage in YJK17 *cdk8-as* strain with or without 20 μM 1-NA-PP1 treatment by western blotting. **E.** A schematic representation of YMV80 single strand annealing repair strain (*36*). The HO-induced break between two homologous *LEU2* sequences (indicated as gray bars) leads to extensive resection of the 25kb sequence between the two homologous sequences. The DNA break is repaired when the exposed homologous sequences anneal. **F.** The viability of CKM deletion mutants in YMV080 strain (n=3, error bars represent S.E.M.). **G.** DNA repair kinetics measured by primer

extension assay in YMV80 *cdk8-as* with and without 20 μM 1-NA-PP1 treatment (n=3, error bars represent S.E.M.). **H.** Rad53 hyperphosphorylation following DNA damage in YMV80 *cdk8-as* strain with or without 20 μM 1-NA-PP1 treatment by western blotting. **I.** Drug sensitivity assay with *cdk8-kd*, *mec1-kd* and *rad53-kd* mutants. All mutants contain *sml1Δ* compensatory mutation for viability, including the WT control strain. 10-fold serially diluted overnight cultures were spotted on YEPD plates containing 5 mM of hydroxyurea or exposed to UV at a concentration of 200 J/m^2 UV after spotting as indicated.

Figure 4. A. Bulk RNA sequencing analysis of Med12-AID cells 8 hours after DNA damage induction by HO endonuclease, and 10 hours CKM depletion by auxin (IAA) treatment. Heatmap of each transcript is plotted as log2 change relative to untreated control. **B.** Log2 fold change values of individual transcripts from Figure 4A. **C.** Western blot analysis of Cdk8-AID-myc, Rad53, Med1-HA, RNAPII subunit Rbp3-V3, RNAPII, RNAPII-S2P, RNAPII-S5P and Pgk1 loading control in *cdk8-as* strain with or without 20 μM 1-NA-PP1 inhibition. Persistent nonspecific bands in Med1-HA blots are annotated with an asterisk (*). **D.** DNA damage responses following auxin-inducible degradation of core Mediator subunits Med14 and Med17, transcription preinitiation subunit Sua7 and the RNAPII subunit Rpo21 and *cdk8-kd* mutant assayed via Rad53 hyperphosphorylation. **E.** DNA damage responses of cdk8-kd strains after the depletion of Med14 and Sua7 monitored via Rad53 hyperphosphorylation.

Figure 5. A. Fold Rbp3-V5 (RNAPII) enrichment in four control loci across the genome with varying levels of Cdk8, RNAPII and Med1 enrichment. Normalized Cdk8, RNAPII and Med1 enrichment values for these loci were obtained from Rossi *et. al* (*50*), and are plotted by using IGV. Below are the fold Rbp3-V5 (RNAPII) enrichment at the same four control loci in a WT strain and a *cdk8-as* strain treated with 20 μM 1-NA-PP1 following DNA damage, measured by chromatin immunoprecipitation of Rbp3-V5 followed by qPCR. Data was normalized to an input sample, a control locus and then to an untreated condition (n=3, error bars represent S.E.M.). **B.** Cell lysates blotted for Rad53, Med13, Med12, Cdk8, CycC and Pgk1 for loading control following DNA damage and IAA treatment to deplete Med13-AID. **C.** Cdk8-FLAG coimmunoprecipitation samples blotted for Cdk8, Med13, Med12, CycC, RNAPII, RNAPII-S2P and RNAPII-S5P before and after DNA damage and Med13-AID depletion by 100 μM auxin treatment. **D.** Med13-myc coimmunoprecipitation samples blotted for Cdk8, Med13, Med12, CycC, RNAPII, RNAPII-S2P and RNAPII-S5P before and after DNA damage and Med13-AID depletion.

Figure 6. A. Enrichment of RNAPII, Cdk8, Med1 and γ-H2AX around an irreparable DNA break assayed by chromatin immunoprecipitation followed by qPCR in WT control strain and *cdk8-as* strain treated with 20 μM 1-NA-PP1. Data was normalized to a control locus, to the input and

then to undamaged control and plotted as normalized fold enrichment (n>2, error bars represent S.E.M.). **B.** Localization of mScarletI epitope-tagged Med17, Cdk8 and CycC in WT and *cdk8-kd* strains in live cells. To induce DNA damage, cells were treated with galactose to induce the expression of HO endonuclease for 8 hours.

Experimental Model and Subject Details

Yeast strains were freshly thawed from frozen stocks and grown at 30^0C using standard practices. Plasmids and yeast strains used in this study are listed in Table S1 and S2. ORF deletions are introduced either through one step PCR homology cassette amplification (*61*) or by using CRISPR/Cas9 as explained previously (*62*). The sequences of template DNAs used for gene targeting experiments are listed in Table S3. Epitope tagged strains were created either by using PCR-amplified homology cassettes (*63*) or by using CRISPR/Cas9 gene targeting methods. The AID tagged strains were constructed as explained previously (*64*).

Method Details

Yeast Media: Yeast strains were grown in YEPD (1% yeast extract, 2% peptone, 2% dextrose, 0.004% adenine pH5.5). For experiments involving a galactose induction, cells were inoculated in YEP containing 3% lactic acid and treated with a final concentration of 2% galactose (Sigma-Aldrich). For the inducible degradation of the proteins, the cultures were treated with 100 µg/ml indole-3-acetic acid (IAA) (Sigma-Aldrich). For inhibition of Cdk8 kinase activity in *cdk8-as* (Y236G) mutant, cells were treated with a final concentration of 10-20 µM 1-NA-PP1 (Cayman Chemical, catalog number 10954-10). Temperature-sensitive conditional mutant *cdc13-1* was grown at permissive temperature (25^0C) and shifted to nonpermissive temperature (33^0C) to induce DNA damage.

Epistatic Miniarray Profiling Screen (E-MAP): The E-MAP screen (*17*) was performed as explained in detail (*27*). The yeast strains used for this assay are listed in Table S2. The E-MAP scores for different genes were plotted by using Cluster (*65*) and TreeView (*66*).

Spot Assays: Cells were grown in YEPD overnight to saturation. Then, they were diluted to a stock concentration of 10^8 cells/ml. Then, cells were serially diluted 10-fold and 2 µl of each dilution was spotted on plates containing 5 mM hydroxyurea (Sigma-Aldrich) or on YEPD and exposed to UV with a dose of 200 J/m^2. Plates were incubated at 30^0C in the dark until colonies formed, and then they were imaged by using Amersham ImageQuant 800. Images were processed by using Fiji (*67*).

Adaptation Assays: Liquid cultures were grown overnight in YEP-lactate. 50 individual G1 cells were micromanipulated on YEP-galactose plates. At various time points, number of adapted cells were scored as a ratio of cells that are past the G2/M arrest stage to total number of cells divided (*1*). For adaptation assays with *cdc13-1* strains, cells were micromanipulated on YEP-dextrose plates and grown at permissive temperature (25^0C) as control or nonpermissive temperature (33^0C) to induce DNA damage.
Viability Assays: The cells were grown in liquid YEP-lactate overnight and micromanipulated on YEP-galactose plates as described above. Viability was calculated as a ratio of microcolonies formed to the total number of cells divided at 24 hours.

HO-induction time course: Overnight YEP-dextrose liquid cultures were washed 3 times with YEP-lactate and were grown in YEP-lactate for 6-8 hours (nearly two doubling times). This saturated culture was then used to inoculate a fresh YEP-lactate culture which was grown to early exponential phase (1-10 10^6 cells/ml). DNA damage was induced by addition of galactose to the media at a final concentration of 2%. For western blot analyses from cell lysates, 50 ml of culture was harvested by centrifugation, washed with 1 ml of 20 % trichloroacetic acid (Sigma-Aldrich) and snap-frozen on dry ice. For coimmunoprecipitation experiments, nearly 500 mg of wet yeast pellet was collected, washed with 1 ml of ice-cold Tris-EDTA buffer (50mM of Tris pH 8.0, 5 mM of EDTA, pH 8.0). For chromatin immunoprecipitation experiments, 45 ml of culture was crosslinked with 1% formaldehyde (Sigma-Aldrich) for 10 minutes at room temperature with gentle shaking. The crosslinking reaction was quenched by addition of glycine at a final concentration of 125 mM and incubation on a platform rocker for 5 minutes at room temperature. After centrifugation, cell pellets were washed 3 times with 1 X TBS (pH 7.4). For RNA sequencing experiments, 50 ml of culture was harvested with centrifugation. The cell pellet was washed with 1 ml of ice-cold water, flash frozen with liquid nitrogen and saved at -80^0C.

Sample preparation for Western Blotting: Whole cell lysate samples were prepared as described (*68*). Briefly, frozen cell pellets were resuspended in 200 µl of 20 % TCA on ice and lysed with vortexing for 3 minutes with acid-wash glass beads (Sigma-Aldrich). The glass beads were washed with 200 µl of 5% TCA twice and the crude extract was collected to a new tube. The crude extract was spun down at 3000 rpm for 10 minutes. The TCA supernatant was discarded, and the protein pellet was resuspended in 200 µl of Laemmli buffer (60 mM Tris, pH 6.8, 2% SDS, 10% glycerol, 0.2 % bromophenol blue, 0.9 % B-mercaptoethanol) and neutralized with 200 µl of Tris (1M, pH 8.0). Prior to loading, the samples were boiled at 95^0C for 5 minutes and spun down for 2 minutes at maximum speed.

Coimmunoprecipitation: Coimmunoprecipitation was performed as previously described (*69*). Frozen cell pellets were resuspended in lysis buffer (50 mM HEPES pH 7.5, 150 mM NaCl, 2 mM EDTA, 0.5% NP-40 supplemented with protease inhibitors. The resuspension was vortexed for 1 hour at 4^0C with acid-washed glass beads for lysis. The extracts were spun down at maximum speed for 10 minutes at 4^0C and the precleared crude lysates were transferred to fresh tubes on ice. Precleared lysates were incubated with Protein A or G-agarose beads (depending on the primary antibody) pre-incubated with the antibody of interest overnight at 4^0C on a rocker platform. Then, the beads were washed 3 times with 1 ml of lysis buffer supplemented with protease inhibitors for 5 minutes. Samples were eluted in 100 µl 6X Laemmli buffer by boiling at 95^0C for 5 minutes. Beads were spun down and the eluates were used for western blotting. The antibodies used for coimmunoprecipitation experiments are listed in Table S4.

Western blotting: Hand-casted polyacrylamide gels were run by using BioRad Mini-PROTEAN tetra cell system in 1X SDS-PAGE buffer, made by diluting the 10 X stock (250 mM Tris, 1.92 M glycine, 1 % SDS in 1000 ml of distilled water). Once the desired protein separation was achieved, the proteins were transferred to Millipore Immobilon-PSQ PVDF membrane at 4^0C by using BioRad Mini Trans-Blot Cell in 1 X transfer buffer containing 100 ml methanol (for 10 X transfer buffer, 250 mM, 1.92 M Glycine in 1000 ml of distilled water). After transfer, the membranes were incubated in 1 X TBS (for 10 X TBS, 200 mM Tris, 1.5 M NaCl in 1000 ml distilled water, pH 7.4 with concentrated HCl) containing 1 ml of Tween-20 (Fisher Scientific) and 5 % dry milk (Fisher Scientific). The primary and secondary antibodies used in this study are listed in Table S4. Membranes were developed by using Amersham Select Western Blot Detection Reagent and visualized by using GE ImageQuant LAS 4000 Biomolecular Imager. BioRad ImageLab software was used to manipulate the images.

Chromatin immunoprecipitation: The samples were collected and cross-linked with a final concentration of 1% formaldehyde, then quenched with glycine at a final concentration of 125 mM, washed 3 times with 1 X TBS (pH 7.4) and snap-frozen on dry ice. To lyse the cells, frozen cell pellets were resuspended on ice in 0.55 ml lysis buffer (50 mM HEPES, pH 7.4, 1mM EDTA, pH 8.0, 140 mM NaCl, 1% Triton X-100, 0.1 % sodium deoxycholate) freshly supplemented with protease inhibitors, 1 mM PMSF and 1 mg/ml bacitracin. Cell pellets were lysed with acid-washed glass beads on a vortexer at 4^0C for 1 hour. Crude cell lysate was harvested and sonicated by using Bioruptor Pico (Diagenode) for 13 cycles (30 seconds on and 30 seconds off). Sonicated cell lysates were cleared by centrifugation at maximum speed for 10 minutes at 4^0C and cleared lysates were transferred to a fresh tube. 50 ul of the crude lysate was set aside as input control, and the rest of the cleared lysate was incubated with the antibody of interest (~1-5 µg) for 1 hour at 4^0C, and subsequently, with Protein A or G agarose beads (50-70 µl) calibrated with lysis buffer for 1 hour at 4^0C. Please see Table S4 for the list of antibodies. After

the incubation, tubes were gently spun down and the unbound lysate was removed with a syringe needle connected to an aspirator. Beads were washed twice with lysis buffer, then with lysis buffer with 500 mM NaCl, wash buffer (10 mM Tris, pH 8.0, 1 mM EDTA, pH 8.0, 0.25 M LiCl, 0.5 % of IGEPAL CA-630, 0.5 % of sodium deoxycholate) and finally with 1 X TE (10 mM Tris, pH 8.0, 1 mM EDTA, pH 8.0). Material bound to the beads was eluted with 100 µl of elution buffer (50 mM Tris, pH 8.0, 1 mM EDTA, pH 8.0, 1% SDS) by incubating the beads at 65^0C for 10 minutes and subsequently with 150 µl of 1 X TE with 0.67 % SDS. Input control samples were supplemented with 200 µl of 1 X TE with 1 % SDS. All samples were treated with 250 µl of 1 X TE and 100 µg of Proteainase K and incubated at 65^0C overnight for the reversal of the crosslinks. The DNA was extracted by using 55 µl of 4 M LiCl and 500 µl of phenol and precipitated by addition of 1 ml of 100 % ethanol and 20 µg of glycogen to the aqueous layer. Samples were incubated at -80^0C for 1 hour, and DNA was precipitated by centrifugation at maximum speed for 10 minutes. DNA pellets were washed with 75 % ethanol twice, and after the evaporation of ethanol, were resuspended in 100 µl of 1 X TE. DNA samples were analyzed by using qPCR.

Real time quantitative PCR: 3 identical reactions were set up for each DNA and primer pair with 2X PowerUp SYBR Green Master Mix (Applied Biosystems cat #A25741) by using BioRad CFX96 thermocyclers. The Cq values for 3 technical replicates were averaged for reach reaction, normalized to a control locus, the input and then to the untreated sample. Results from independent experiments were plotted by using Prism 9 (Graphpad). The primer sets used for the qPCR assays are listed in Table S5. Other primer sequences are available upon request.

Measurement of DNA repair kinetics: 50 ml of yeast cultures were harvested at various time points and snap-frozen on dry ice as explained above. DNA was extracted by using MasterPure Yeast DNA purification kit (Biosearch Technologies, cat # MPY80200). The DNA samples were quantified and diluted. Primer pairs targeting the repair product and a control locus were used to set up PCRs. The PCR products were then on agarose gels, visualized by using Amersham ImageQuant 800 and quantified by using BioRad ImageLab software. The results from 3 separate experiments were averaged and plotted by using Prism 9 (Graphpad).

RNA extraction, library preparation and RNA sequencing: Yeast cultures were grown and harvested as explained above and snap frozen on dry ice. RNA was extracted by using the RiboPure RNA extraction kit (ThermoFisher, cat # AM1926), ERCC spike-in mix was added to each sample for normalization. The samples were run on 2100 Bioanalyzer (Agilent) for quality control. Sequencing libraries were prepared by using Illumina Stranded mRNA Prep and sequenced by using Illumina NovaSEQ 6000 platform (100 base, paired end). Duplicate reads were removed and the adapter sequences were clipped by using Trimmomatic (*70*). Paired end reads were catenated and aligned to SacCer3 reference yeast genome by using STAR (*71*). The

SAM files were converted to BAM, and the reads were sorted by using Samtools. The read numbers were extracted by using QoRTs (*72*), and the reads were normalized to ERCC Spike-in controls. Lastly, the reads were normalized to an untreated condition and plotted by using Cluster and Treeview.

Live cell imaging: Overnight yeast cultures were grown in YEP-lac at 30^0C. To induce DNA damage, cultures were treated with a final concentration of 2 % galactose for 8 hours to allow full activation of DNA damage response. Prior to imaging, the cultures were washed into synthetic complete media 3 times and finally resuspended in synthetic media. Cultures were imaged by using Olympus IX81 confocal microscope with a 100 X 1.45 PlanApo lens. The images were manipulated by using FiJi (*67*).

Availability of data and materials

RNA sequencing data generated for this study will be made available at the Gene Expression Omnibus (GEO) after peer review. All data and materials are available upon request (email: gonen@uchicago.edu; aruthenburg@uchicago.edu)

Competing interests

Authors declare no competing interests.

Funding

G. M. is supported by the NIH Ruth L. Kirschtein National Research Service Award (NRSA) (F32GM145156) and The University of Chicago Women's Board Grant Fund. This work is supported by NIH grant R35GM145373 to A.J.R.

Acknowledgements

We thank Douglas Bishop lab for reagents, equipment and for useful suggestions.

References

1. S. E. Lee *et al.*, Saccharomyces Ku70, mre11/rad50 and RPA proteins regulate adaptation to G2/M arrest after DNA damage. *Cell* **94**, 399-409 (1998).
2. H. Neecke, G. Lucchini, M. P. Longhese, Cell cycle progression in the presence of irreparable DNA damage is controlled by a Mec1- and Rad53-dependent checkpoint in budding yeast. *Embo j* **18**, 4485-4497 (1999).
3. Y. Sanchez *et al.*, Regulation of RAD53 by the ATM-like kinases MEC1 and TEL1 in yeast cell cycle checkpoint pathways. *Science* **271**, 357-360 (1996).

4. P. Pizzul *et al.*, The DNA damage checkpoint: A tale from budding yeast. *Front Genet* **13**, 995163 (2022).
5. R. Kato, H. Ogawa, An essential gene, ESR1, is required for mitotic cell growth, DNA repair and meiotic recombination in Saccharomyces cerevisiae. *Nucleic Acids Res* **22**, 3104-3112 (1994).
6. R. S. Cha, N. Kleckner, ATR homolog Mec1 promotes fork progression, thus averting breaks in replication slow zones. *Science* **297**, 602-606 (2002).
7. J. A. Tercero, J. F. Diffley, Regulation of DNA replication fork progression through damaged DNA by the Mec1/Rad53 checkpoint. *Nature* **412**, 553-557 (2001).
8. C. Santocanale, J. F. Diffley, A Mec1- and Rad53-dependent checkpoint controls late-firing origins of DNA replication. *Nature* **395**, 615-618 (1998).
9. X. Zhao, E. G. Muller, R. Rothstein, A suppressor of two essential checkpoint genes identifies a novel protein that negatively affects dNTP pools. *Mol Cell* **2**, 329-340 (1998).
10. F. M. Bastos de Oliveira *et al.*, Phosphoproteomics reveals distinct modes of Mec1/ATR signaling during DNA replication. *Mol Cell* **57**, 1124-1132 (2015).
11. M. C. Lanz *et al.*, Separable roles for Mec1/ATR in genome maintenance, DNA replication, and checkpoint signaling. *Genes Dev* **32**, 822-835 (2018).
12. A. Gunjan, A. Verreault, A Rad53 kinase-dependent surveillance mechanism that regulates histone protein levels in S. cerevisiae. *Cell* **115**, 537-549 (2003).
13. O. Tsaponina, E. Barsoum, S. U. Astrom, A. Chabes, Ixr1 is required for the expression of the ribonucleotide reductase Rnr1 and maintenance of dNTP pools. *PLoS Genet* **7**, e1002061 (2011).
14. Y. J. Sheu, R. K. Kawaguchi, J. Gillis, B. Stillman, Prevalent and dynamic binding of the cell cycle checkpoint kinase Rad53 to gene promoters. *Elife* **11**, (2022).
15. B. Ho, E. J. Sanford, N. P. Torres, M. B. Smolka, G. W. Brown, Mec1-Independent Activation of the Rad53 Checkpoint Kinase Revealed by Quantitative Analysis of Protein Localization Dynamics. *bioRxiv*, 2022.2008.2004.502543 (2022).
16. M. Schuldiner, S. R. Collins, J. S. Weissman, N. J. Krogan, Quantitative genetic analysis in Saccharomyces cerevisiae using epistatic miniarray profiles (E-MAPs) and its application to chromatin functions. *Methods* **40**, 344-352 (2006).
17. M. Schuldiner *et al.*, Exploration of the function and organization of the yeast early secretory pathway through an epistatic miniarray profile. *Cell* **123**, 507-519 (2005).
18. W. F. Richter, S. Nayak, J. Iwasa, D. J. Taatjes, The Mediator complex as a master regulator of transcription by RNA polymerase II. *Nature Reviews Molecular Cell Biology*, (2022).
19. M. R. Dotson *et al.*, Structural organization of yeast and mammalian mediator complexes. *Proc Natl Acad Sci U S A* **97**, 14307-14310 (2000).
20. F. J. Asturias, Y. W. Jiang, L. C. Myers, C. M. Gustafsson, R. D. Kornberg, Conserved structures of mediator and RNA polymerase II holoenzyme. *Science* **283**, 985-987 (1999).
21. Y. Liu, J. A. Ranish, R. Aebersold, S. Hahn, Yeast nuclear extract contains two major forms of RNA polymerase II mediator complexes. *J Biol Chem* **276**, 7169-7175 (2001).
22. S.-M. Liao *et al.*, A kinase–cyclin pair in the RNA polymerase II holoenzyme. *Nature* **374**, 193-196 (1995).

23. M. T. Knuesel, K. D. Meyer, A. J. Donner, J. M. Espinosa, D. J. Taatjes, The Human CDK8 Subcomplex Is a Histone Kinase That Requires Med12 for Activity and Can Function Independently of Mediator. *Molecular and Cellular Biology* **29**, 650-661 (2009).
24. L. C. Myers *et al.*, The Med proteins of yeast and their function through the RNA polymerase II carboxy-terminal domain. *Genes Dev* **12**, 45-54 (1998).
25. J. Anandhakumar, Y. W. Moustafa, S. Chowdhary, A. S. Kainth, D. S. Gross, Evidence for Multiple Mediator Complexes in Yeast Independently Recruited by Activated Heat Shock Factor. *Mol Cell Biol* **36**, 1943-1960 (2016).
26. J. Nemet, B. Jelicic, I. Rubelj, M. Sopta, The two faces of Cdk8, a positive/negative regulator of transcription. *Biochimie* **97**, 22-27 (2014).
27. S. R. Collins, A. Roguev, N. J. Krogan, Quantitative genetic interaction mapping using the E-MAP approach. *Methods Enzymol* **470**, 205-231 (2010).
28. J. Majka, P. M. Burgers, Yeast Rad17/Mec3/Ddc1: a sliding clamp for the DNA damage checkpoint. *Proc Natl Acad Sci U S A* **100**, 2249-2254 (2003).
29. F. D. Sweeney *et al.*, Saccharomyces cerevisiae Rad9 acts as a Mec1 adaptor to allow Rad53 activation. *Curr Biol* **15**, 1364-1375 (2005).
30. P. Zheng *et al.*, SPK1 is an essential S-phase-specific gene of Saccharomyces cerevisiae that encodes a nuclear serine/threonine/tyrosine kinase. *Mol Cell Biol* **13**, 5829-5842 (1993).
31. V. Paciotti, M. Clerici, M. Scotti, G. Lucchini, M. P. Longhese, Characterization of mec1 kinase-deficient mutants and of new hypomorphic mec1 alleles impairing subsets of the DNA damage response pathway. *Mol Cell Biol* **21**, 3913-3925 (2001).
32. S. M. Liao *et al.*, A kinase-cyclin pair in the RNA polymerase II holoenzyme. *Nature* **374**, 193-196 (1995).
33. R. Anand, G. Memisoglu, J. Haber, Cas9-mediated gene editing in Saccharomyces cerevisiae. (2017).
34. S. E. Lee *et al.*, Arrest, adaptation, and recovery following a chromosome double-strand break in Saccharomyces cerevisiae. *Cold Spring Harb Symp Quant Biol* **65**, 303-314 (2000).
35. B. Garvik, M. Carson, L. Hartwell, Single-stranded DNA arising at telomeres in cdc13 mutants may constitute a specific signal for the RAD9 checkpoint. *Mol Cell Biol* **15**, 6128-6138 (1995).
36. M. B. Vaze *et al.*, Recovery from checkpoint-mediated arrest after repair of a double-strand break requires Srs2 helicase. *Mol Cell* **10**, 373-385 (2002).
37. P. Kemmeren *et al.*, Large-scale genetic perturbations reveal regulatory networks and an abundance of gene-specific repressors. *Cell* **157**, 740-752 (2014).
38. K. Nishimura, T. Fukagawa, H. Takisawa, T. Kakimoto, M. Kanemaki, An auxin-based degron system for the rapid depletion of proteins in nonplant cells. *Nat Methods* **6**, 917-922 (2009).
39. Y. Liu *et al.*, Two cyclin-dependent kinases promote RNA polymerase II transcription and formation of the scaffold complex. *Mol Cell Biol* **24**, 1721-1735 (2004).
40. M. C. Keogh *et al.*, A phosphatase complex that dephosphorylates gammaH2AX regulates DNA damage checkpoint recovery. *Nature* **439**, 497-501 (2006).

41. A. Mehta, A. Beach, J. E. Haber, Homology Requirements and Competition between Gene Conversion and Break-Induced Replication during Double-Strand Break Repair. *Mol Cell* **65**, 515-526.e513 (2017).
42. C. I. White, J. E. Haber, Intermediates of recombination during mating type switching in Saccharomyces cerevisiae. *Embo j* **9**, 663-673 (1990).
43. F. Eyboulet *et al.*, Mediator links transcription and DNA repair by facilitating Rad2/XPG recruitment. *Genes Dev* **27**, 2549-2562 (2013).
44. D. Gopaul *et al.*, Genome-wide distribution of Rad26 and Rad1-Rad10 reveals their relationship with Mediator and RNA polymerase II. *bioRxiv*, 2021.2010.2020.465181 (2021).
45. S. Osman *et al.*, The Cdk8 kinase module regulates interaction of the mediator complex with RNA polymerase II. *J Biol Chem* **296**, 100734 (2021).
46. A. Tufegdžić Vidaković *et al.*, Regulation of the RNAPII Pool Is Integral to the DNA Damage Response. *Cell* **180**, 1245-1261.e1221 (2020).
47. K. L. Tsai *et al.*, Subunit Architecture and Functional Modular Rearrangements of the Transcriptional Mediator Complex. *Cell* **158**, 463 (2014).
48. C. Plaschka *et al.*, Architecture of the RNA polymerase II-Mediator core initiation complex. *Nature* **518**, 376-380 (2015).
49. J. P. Tourigny, K. Schumacher, M. M. Saleh, D. Devys, G. E. Zentner, Architectural Mediator subunits are differentially essential for global transcription in Saccharomyces cerevisiae. *Genetics*, (2021).
50. M. J. Rossi *et al.*, A high-resolution protein architecture of the budding yeast genome. *Nature* **592**, 309-314 (2021).
51. S. Egloff, S. Murphy, Cracking the RNA polymerase II CTD code. *Trends Genet* **24**, 280-288 (2008).
52. C. J. Hengartner *et al.*, Temporal regulation of RNA polymerase II by Srb10 and Kin28 cyclin-dependent kinases. *Mol Cell* **2**, 43-53 (1998).
53. S. R. Collins *et al.*, Functional dissection of protein complexes involved in yeast chromosome biology using a genetic interaction map. *Nature* **446**, 806-810 (2007).
54. R. Shroff *et al.*, Distribution and dynamics of chromatin modification induced by a defined DNA double-strand break. *Curr Biol* **14**, 1703-1711 (2004).
55. K.-L. Tsai *et al.*, A conserved Mediator–CDK8 kinase module association regulates Mediator–RNA polymerase II interaction. *Nature Structural & Molecular Biology* **20**, 611-619 (2013).
56. A. S. Adler *et al.*, CDK8 maintains tumor dedifferentiation and embryonic stem cell pluripotency. *Cancer Res* **72**, 2129-2139 (2012).
57. M. H. Hofmann *et al.*, Selective and Potent CDK8/19 Inhibitors Enhance NK-Cell Activity and Promote Tumor Surveillance. *Mol Cancer Ther* **19**, 1018-1030 (2020).
58. E. M. Schleicher *et al.*, Dual genome-wide CRISPR knockout and CRISPR activation screens identify mechanisms that regulate the resistance to multiple ATR inhibitors. *PLoS Genet* **16**, e1009176 (2020).
59. R. L. Lloyd *et al.*, Loss of Cyclin C or CDK8 provides ATR inhibitor resistance by suppressing transcription-associated replication stress. *Nucleic Acids Res* **49**, 8665-8683 (2021).

60. B. Guglielmi *et al.*, A high resolution protein interaction map of the yeast Mediator complex. *Nucleic Acids Res* **32**, 5379-5391 (2004).
61. A. Wach, A. Brachat, R. Pohlmann, P. Philippsen, New heterologous modules for classical or PCR-based gene disruptions in Saccharomyces cerevisiae. *Yeast* **10**, 1793-1808 (1994).
62. R. Anand, G. Memisoglu, J. E. Haber, *Protocol Exchange*, (2020).
63. M. S. Longtine *et al.*, Additional modules for versatile and economical PCR-based gene deletion and modification in Saccharomyces cerevisiae. *Yeast* **14**, 953-961 (1998).
64. M. Morawska, H. D. Ulrich, An expanded tool kit for the auxin-inducible degron system in budding yeast. *Yeast* **30**, 341-351 (2013).
65. M. B. Eisen, P. T. Spellman, P. O. Brown, D. Botstein, Cluster analysis and display of genome-wide expression patterns. *Proc Natl Acad Sci U S A* **95**, 14863-14868 (1998).
66. A. J. Saldanha, Java Treeview—extensible visualization of microarray data. *Bioinformatics* **20**, 3246-3248 (2004).
67. J. Schindelin *et al.*, Fiji: an open-source platform for biological-image analysis. *Nature Methods* **9**, 676-682 (2012).
68. A. Pellicioli, S. E. Lee, C. Lucca, M. Foiani, J. E. Haber, Regulation of Saccharomyces Rad53 checkpoint kinase during adaptation from DNA damage-induced G2/M arrest. *Mol Cell* **7**, 293-300 (2001).
69. G. Memisoglu *et al.*, Mec1(ATR) Autophosphorylation and Ddc2(ATRIP) Phosphorylation Regulates DNA Damage Checkpoint Signaling. *Cell Rep* **28**, 1090-1102.e1093 (2019).
70. A. M. Bolger, M. Lohse, B. Usadel, Trimmomatic: a flexible trimmer for Illumina sequence data. *Bioinformatics* **30**, 2114-2120 (2014).
71. A. Dobin *et al.*, STAR: ultrafast universal RNA-seq aligner. *Bioinformatics* **29**, 15-21 (2013).
72. S. W. Hartley, J. C. Mullikin, QoRTs: a comprehensive toolset for quality control and data processing of RNA-Seq experiments. *BMC Bioinformatics* **16**, 224 (2015).

Figure 1.

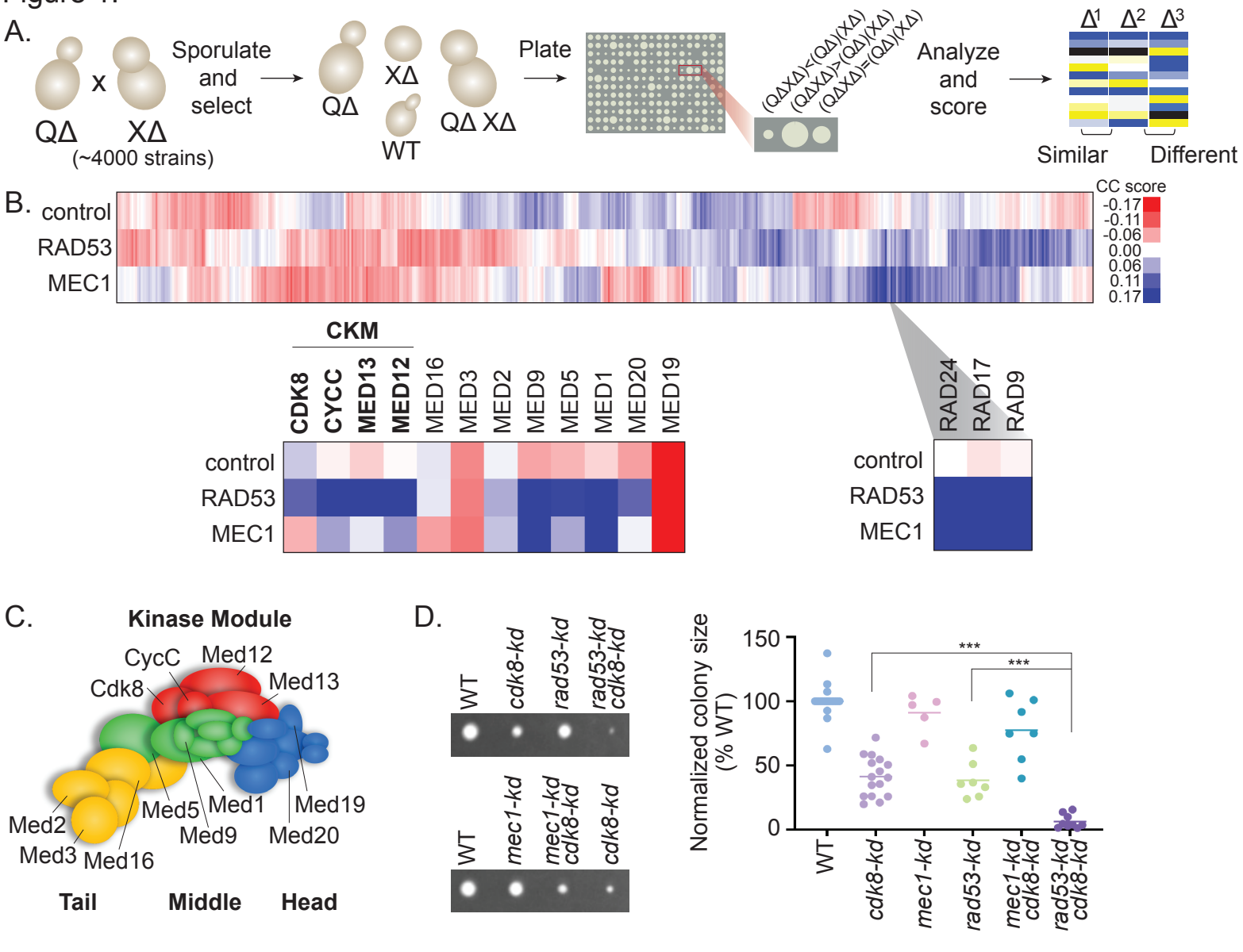
A.
QΔ
x
XΔ
(~4000 strains)
Sporulate and select
QΔ
XΔ
WT
QΔ XΔ
Plate
(QΔXΔ)<(QΔ)(XΔ)
(QΔXΔ)>(QΔ)(XΔ)
(QΔXΔ)=(QΔ)(XΔ)
Analyze and score
Δ1 Δ2 Δ3
Similar
Different
B.
control
RAD53
MEC1
CC score
-0.17
-0.11
-0.06
0.00
0.06
0.11
0.17
CKM
CDK8
CYCC
MED13
MED12
MED16
MED3
MED2
MED9
MED5
MED1
MED20
MED19
RAD24
RAD17
RAD9
C.
Kinase Module
CycC
Med12
Cdk8
Med13
Med2
Med3
Med16
Med5
Med1
Med9
Med19
Med20
Tail
Middle
Head
D.
WT
cdk8-kd
rad53-kd
rad53-kd cdk8-kd
mec1-kd
mec1-kd cdk8-kd
Normalized colony size (% WT)
150
100
50
0
***
***

Figure 2.

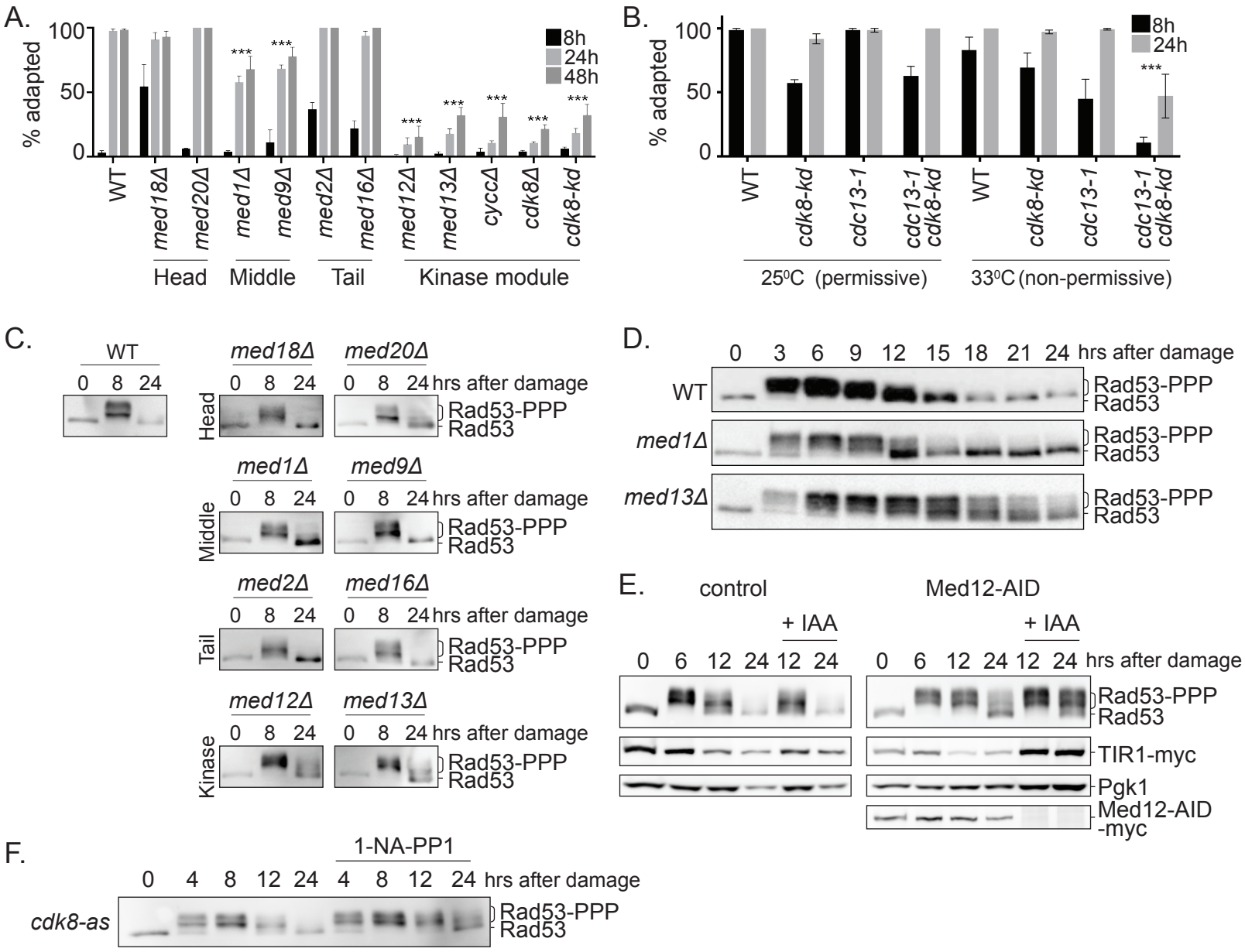
A.
% adapted
100
50
0
8h
24h
48h
***
WT
med18Δ
med20Δ
med1Δ
med9Δ
med2Δ
med16Δ
med12Δ
med13Δ
cycCΔ
cdk8Δ
cdk8-kd
Head
Middle
Tail
Kinase module
B.
% adapted
100
50
0
8h
24h
***
WT
cdk8-kd
cdc13-1
cdc13-1 cdk8-kd
25⁰C (permissive)
33⁰C (non-permissive)
C.
WT
0 8 24
med18Δ
med20Δ
0 8 24 hrs after damage
Head
Rad53-PPP
Rad53
med1Δ
med9Δ
Middle
med2Δ
med16Δ
Tail
med12Δ
med13Δ
Kinase
D.
0 3 6 9 12 15 18 21 24 hrs after damage
WT
med1Δ
med13Δ
Rad53-PPP
Rad53
E.
control
Med12-AID
+ IAA
0 6 12 24 12 24 hrs after damage
Rad53-PPP
Rad53
TIR1-myc
Pgk1
Med12-AID
-myc
F.
1-NA-PP1
0 4 8 12 24 4 8 12 24 hrs after damage
cdk8-as
Rad53-PPP
Rad53

Figure 3.

A. Gene Conversion (YJK17)

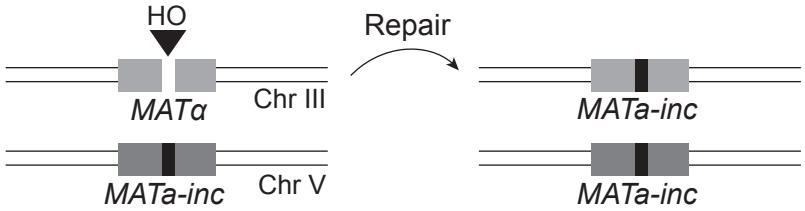

B.

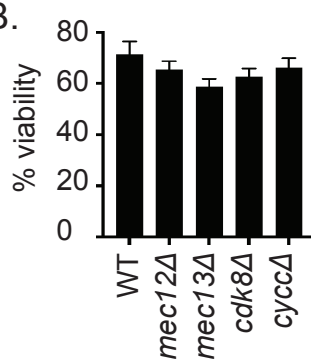

C.

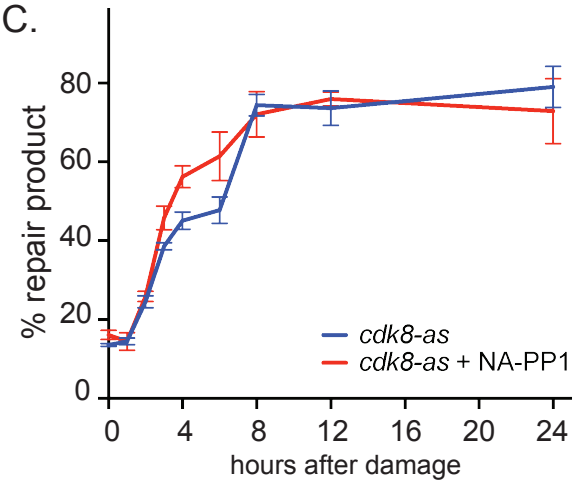

D.

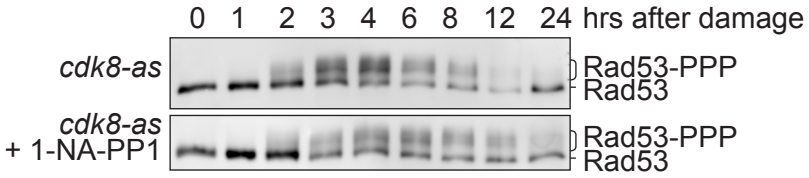

E. Single Strand Annealing (YMV80)

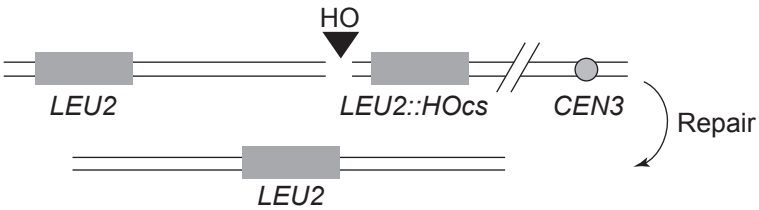

F.

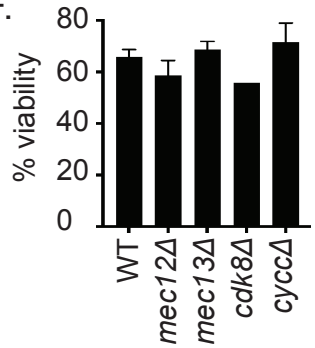

G.

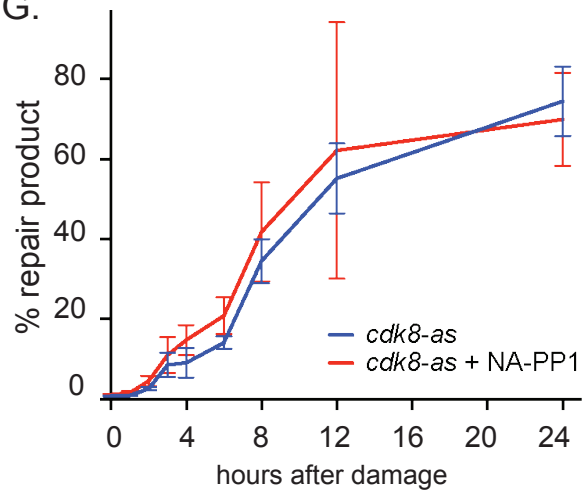

H.

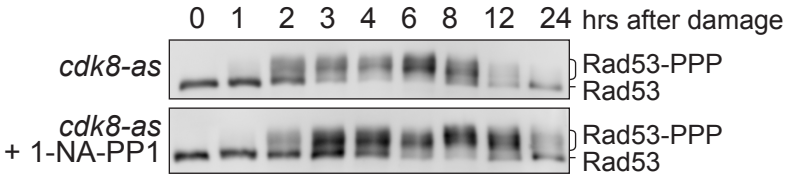

I.

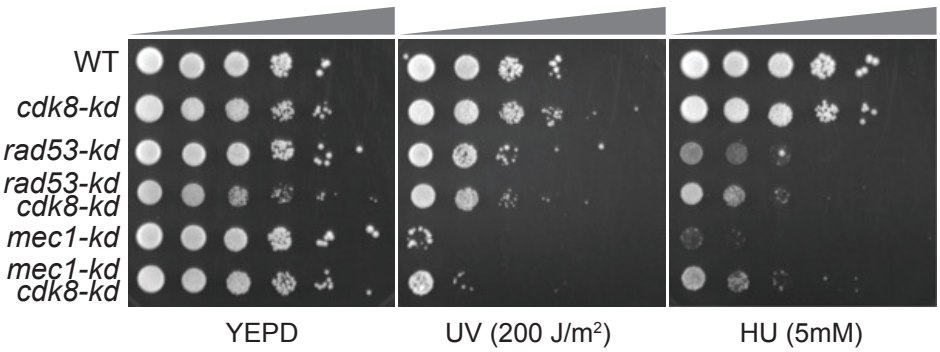

Figure 4.

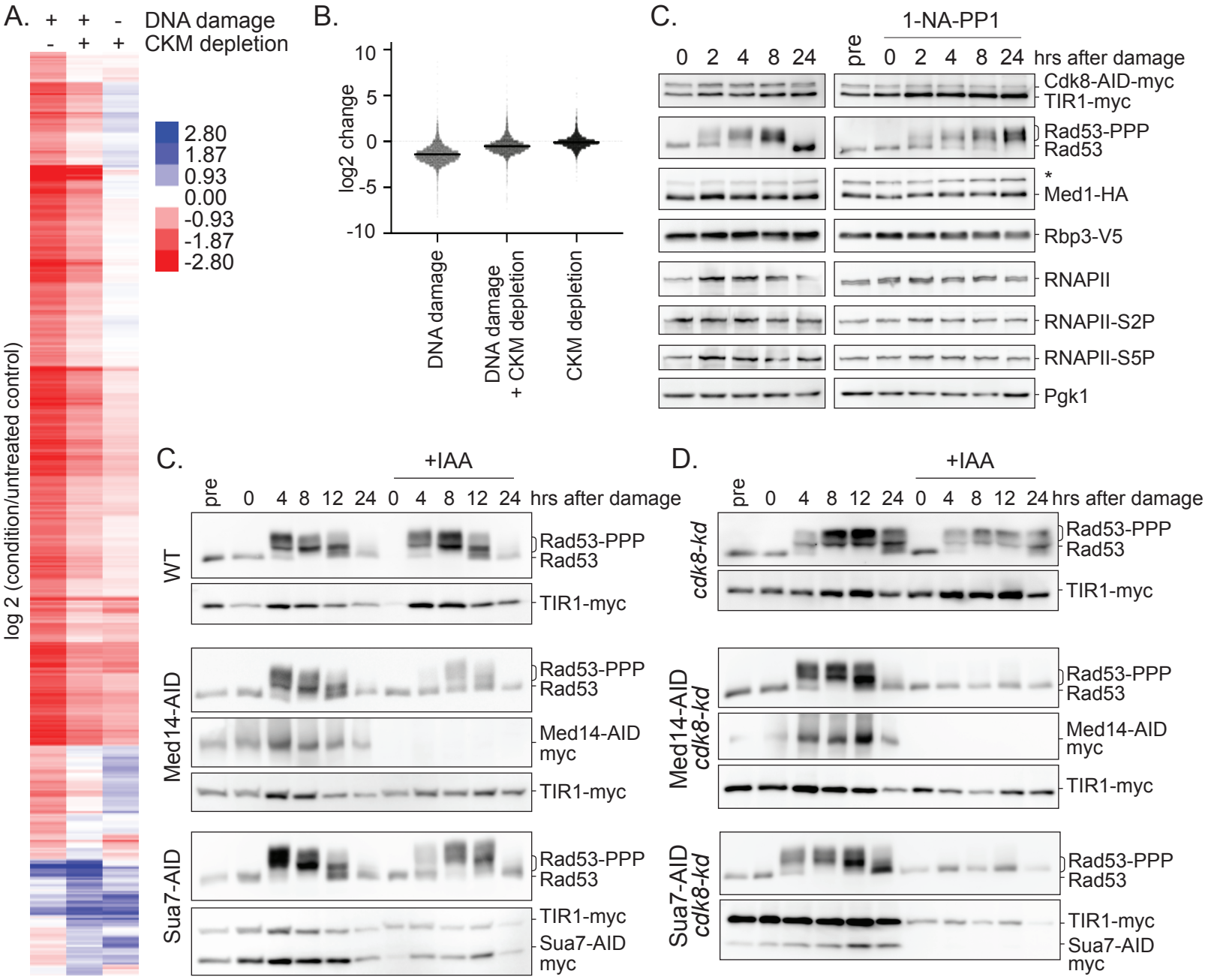
A.
DNA damage
CKM depletion
2.80
1.87
0.93
0.00
-0.93
-1.87
-2.80
log 2 (condition/untreated control)
B.
log2 change
DNA damage
DNA damage + CKM depletion
CKM depletion
C.
1-NA-PP1
hrs after damage
Cdk8-AID-myc
TIR1-myc
Rad53-PPP
Rad53
Med1-HA
Rbp3-V5
RNAPII
RNAPII-S2P
RNAPII-S5P
Pgk1
C.
+IAA
hrs after damage
WT
Med14-AID
Sua7-AID
Rad53-PPP
Rad53
TIR1-myc
Med14-AID myc
Sua7-AID myc
D.
+IAA
hrs after damage
cdk8-kd
Med14-AID cdk8-kd
Sua7-AID cdk8-kd

Figure 5.

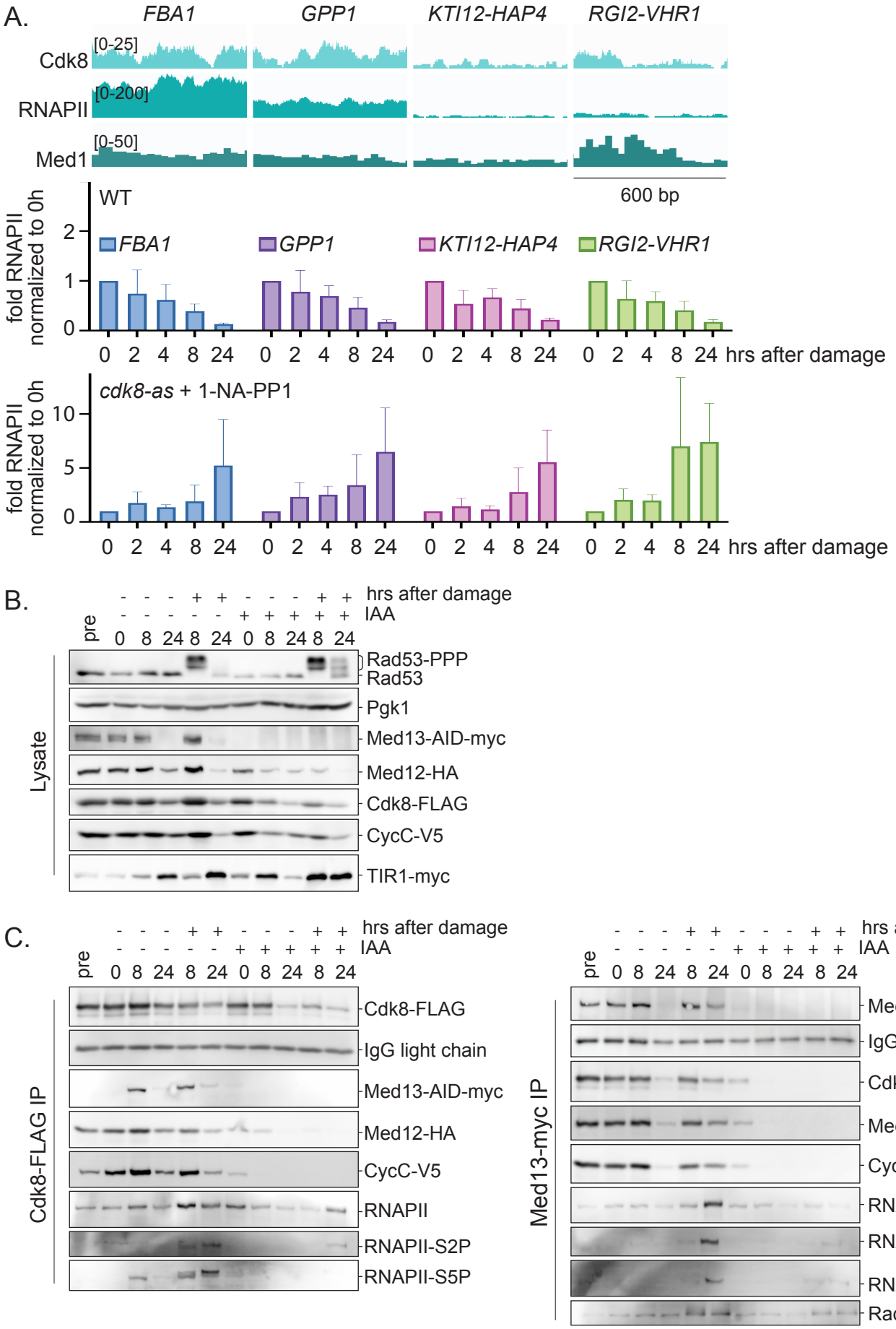
A.
FBA1
GPP1
KTI12-HAP4
RGI2-VHR1
Cdk8
[0-25]
RNAPII
[0-200]
Med1
[0-50]
600 bp
WT
fold RNAPII normalized to 0h
FBA1
GPP1
KTI12-HAP4
RGI2-VHR1
0 2 4 8 24 hrs after damage
cdk8-as + 1-NA-PP1
B.
hrs after damage
IAA
pre
Lysate
Rad53-PPP
Rad53
Pgk1
Med13-AID-myc
Med12-HA
Cdk8-FLAG
CycC-V5
TIR1-myc
C.
Cdk8-FLAG IP
IgG light chain
RNAPII
RNAPII-S2P
RNAPII-S5P
Med13-myc IP
Rad53

Figure 6.

A.

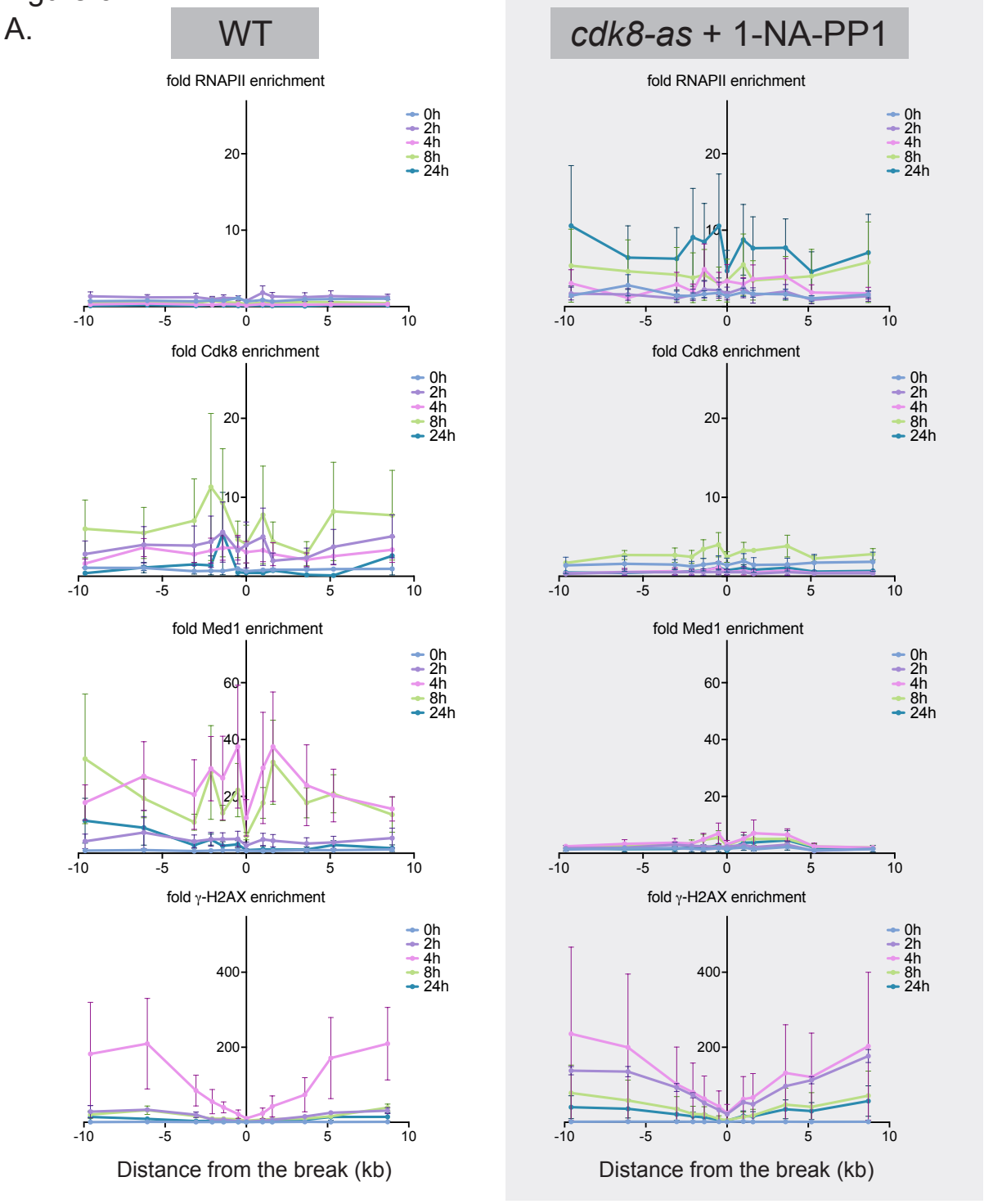
WT
cdk8-as + 1-NA-PP1
fold RNAPII enrichment
fold Cdk8 enrichment
fold Med1 enrichment
fold γ-H2AX enrichment
0h
2h
4h
8h
24h
Distance from the break (kb)

B.

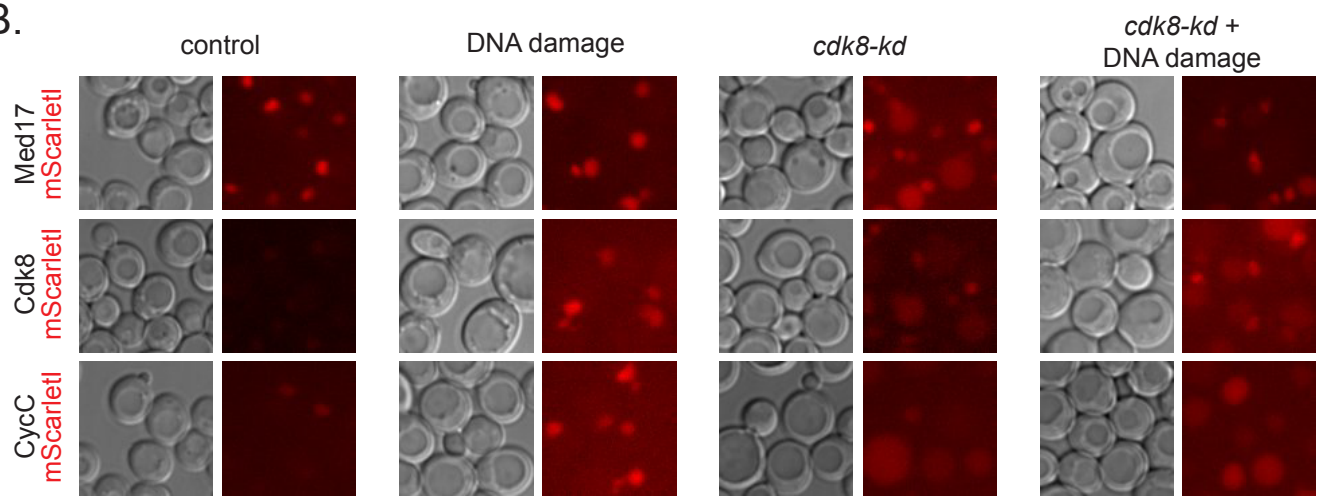
control
DNA damage
cdk8-kd
cdk8-kd + DNA damage
Med17 mScarletI
Cdk8 mScarletI
CycC mScarletI